JVI Accepted Manuscript Posted Online 13 March 2019
J. Virol. doi:10.1128/JVI.00015-19

The Infectious Bronchitis Coronavirus Envelope Protein Alters Golgi pH to Protect Spike Protein and Promote Release of Infectious Virus

Jason W. Westerbeck [1], Carolyn E. Machamer [*]

Department of Cell Biology, The Johns Hopkins University School of Medicine, Baltimore, MD, USA.

* Correspondence should be addressed to Carolyn E. Machamer, machamer@jhmi.edu

[1] Current address: W. Harry Feinstone Department of Molecular Microbiology and Immunology, The Johns Hopkins Bloomberg School of Public Health, Baltimore, MD, USA.

Running title: IBV E neutralizes Golgi pH

Abstract

Coronaviruses (CoVs) assemble by budding into the lumen of the early Golgi prior to exocytosis. The small CoV envelope (E) protein plays roles in assembly, virion release, and pathogenesis. CoV E has a single hydrophobic domain (HD), is targeted to Golgi membranes, and has cation channel activity *in vitro*. The E protein from the avian infectious bronchitis virus (IBV) has dramatic effects on the secretory system, which require residues in the HD. Mutation of the HD of IBV E in a recombinant virus background results in impaired growth kinetics, impaired release of infectious virions, accumulation of IBV spike (S) protein on the plasma membrane when compared IBV WT infected cells, and aberrant cleavage of IBV S on virions. We previously reported the formation of two distinct oligomeric pools of IBV E in transfected and infected cells. Disruption of the secretory pathway by IBV E correlates with a form that is likely monomeric, suggesting that the effects on the secretory pathway are independent of E ion channel activity. Here, we present evidence suggesting that the monomeric form of IBV E correlates with an increased Golgi luminal pH. Infection with IBV or expression of IBV E induces neutralization of Golgi pH, promoting a model in which IBV E alters the secretory pathway through interaction with host cell factors, protecting IBV S from premature cleavage and leading to the efficient release of infectious virus from the cells. This is the first demonstration of a coronavirus-induced alteration in the microenvironment of the secretory pathway.

Importance

Coronaviruses are important human pathogens with significant zoonotic potential. Progress has been made toward identifying potential vaccine candidates for highly pathogenic human CoVs, including use of attenuated viruses that lack the CoV E protein or express E mutants. However, no approved vaccines or anti-viral therapeutics exist. Understanding the role of the CoV E protein in virus assembly and release is thus an important prerequisite to potential vaccines as well as in identifying novel antiviral therapeutics.

Introduction

The majority of human coronaviruses (CoVs) cause mild disease phenotypes. However, when novel coronaviruses like severe acute respiratory syndrome (SARS)-CoV and Middle East respiratory syndrome (MERS)-CoV emerge from their animal reservoirs to infect humans (1) they elicit a robust and aberrant immune response that can lead to a very serious and deadly pneumonia (2). Importantly, there are no effective vaccines or therapeutics to treat these CoVs. Efforts to develop long-term therapeutic strategies to combat novel, highly pathogenic CoVs will be aided by increased understanding of conserved viral mechanisms at the level of their cell and molecular biology.

One of the more fascinating and enigmatic aspects of CoV biology is that CoV virions bud into the lumen of the secretory pathway at the endoplasmic reticulum-Golgi intermediate compartment (ERGIC), and then must navigate through the Golgi and the anterograde endomembrane system to be efficiently released from the host cell (3). The structure and function of the Golgi depends upon an acidic pH gradient that decreases from the lumen of the *cis*-Golgi to the lumen of the *trans*-Golgi. This pH gradient is produced by a balance maintained by proton influx into the lumen of the Golgi, proton leak, and counter-ion conductance (4). Pharmacological and other manipulations of the pH gradient that result in neutralization of the lumen have all been shown to cause slow trafficking of cargo through the Golgi as well as alteration in Golgi morphology (4–7). A class of small viral membrane proteins with ion channel activity, called viroporins (8), have been shown to have dramatic effects on the secretory pathway, similar to those elicited by pharmacological manipulation of luminal pH. Several well-studied members of this viroporin family of proteins include the Influenza A M2 protein (IAV M2), hepatitis C virus (HCV) p7 protein, and the CoV envelope (E) protein. These representative viroporins demonstrate several common functional features despite differences in viral assembly and budding locations. It has been suggested the role of M2 in the secretory pathway is to neutralize luminal pH to protect the HA fusion protein of influenza from premature activation

(9–11). Overexpression of M2 causes secretory pathway disruption where the rate of intracellular trafficking is slowed and Golgi morphology is altered (5). HCV p7 is also thought to play a protective role by allowing egress of viral structural proteins through the secretory pathway. HCV lacking active p7 can be partially rescued by both pharmacological neutralization of the luminal spaces by bafilomycin A1 and by *in trans* expression of IAV M2 (12, 13). Similar to M2, the infectious bronchitis virus (IBV) coronavirus E protein elicits multiple secretory pathway disruption phenotypes when overexpressed in mammalian cells (15).

To understand CoV E at a cell biological level, a recombinant virus system was used to replace the hydrophobic domain (HD) of IBV E with the HD of the vesicular stomatitis virus glycoprotein (VSV G), and the recombinant virus was called IBV-EG3 (14, 15). Replacing the HD of IBV E with a heterologous sequence of the same length does not impair Golgi targeting or interaction with IBV M during assembly (16, 17), but would be expected to impair ion channel function. One-step growth curves revealed that IBV EG3 virus grew to a titer 10-fold lower than IBV WT virus in infected Vero cells. At late times post-infection, the majority of infectious virus resides in the supernatant surrounding IBV WT infected cells, while the majority of infectious IBV EG3 virus is intracellular (14). Vero cells infected with IBV EG3 accumulate more IBV S protein on the plasma membrane than IBV WT infected cells and this accumulation of IBV S leads to an increase in the size and rate of formation of the virus-induced syncytia (14). Highly purified virions from IBV EG3 infected cells lack a full complement of spikes and most S is cleaved near the virion envelope, likely explaining the reduced infectivity of released particles (15). A build-up of vacuole-like compartments containing virions as well as other aberrant material in IBV EG3 infected cells may explain the damage to S (14, 15).

Intriguingly, when IBV WT E is transiently overexpressed in HeLa cells, the Golgi complex completely disassembles while the Golgi in cells overexpressing IBV EG3 is intact (14). This observation suggested that IBV E alters the secretory pathway of the host cell. Expression of IBV E or EG3 reduces trafficking rates of both membrane and secretory cargo (14). Given

that release of infectious IBV EG3 is reduced, it was surprising that wild-type E protein reduced cargo trafficking. We hypothesized that since the HD was required for these phenotypes, alteration of the Golgi lumen by E ion channel activity was required for maintaining intact virus, and the reduced rates of trafficking were an acceptable compromise for the virus (18).

Studies probing the nature of CoV E ion channel activity have centered on understanding the residues required for this activity and the associated pathogenic and cell biological phenotypes elicited by different CoV E proteins. Two residues in the HD of SARS-CoV E, N15 and V25, have been shown to promote viral fitness during infection (19, 20). Mutation of N15 or V25 abolishes ion-channel activity of SARS-CoV E in artificial membranes (19, 20). We previously reported that the E protein of IBV expressed in mammalian cells is found in two pools by velocity gradient analysis: a low molecular weight pool (LMW) and a high molecular weight pool (HMW) (21). The LMW pool represents IBV E in a monomeric state while the HMW pool correlates with a homo-oligomer of IBV E. When mutations corresponding to the conserved HD residues of SARS-CoV E that inhibit ion channel activity were made in IBV E (T16A and A26F), the HD mutants segregate primarily into one oligomeric pool or the other. The E^{T16A} mutant is primarily in the HMW pool while the E^{A26F} mutant is primarily in the LMW pool. The presence of the LMW pool of IBV E, the predominant and likely monomeric form found when E^{A26F} is present, correlates with the secretory pathway disruption associated with the WT IBV E protein (21). This was surprising in that it suggested an E ion channel-independent role for IBV E associated with manipulation of the secretory pathway. It was recently reported that that these HD mutants do abolish ion channel activity of IBV E in artificial membranes, and virus titers are reduced by a log in the supernatant of infected cells, suggesting a defect in virion release (22). Our data on the IBV-EG3 virus corroborates this study (14).

Herein, we provide evidence for the neutralization of Golgi luminal pH during IBV infection and we demonstrate that transient overexpression of the IBV E protein, but not HD mutants deficient in the LMW pool of IBV E, is sufficient to cause a significant increase in the pH

of the Golgi lumen. We suggest that increased trafficking and altered cleavage of the IBV S protein observed during IBV EG3 infection may reflect the detrimental effect of normal Golgi pH on IBV S processing. We demonstrate that IBV S processing and trafficking is similarly aberrant when co-expressed with EG3 or E^{T16A} but not WT E or E^{A26F}, and that IAV M2 can substitute for WT E to protect S from premature cleavage. Our results describe the first demonstration of a coronavirus-mediated alternation of the luminal microenvironment of the secretory pathway.

Results

IBV S is aberrantly processed in EG3 virions.

The IBV S protein is cleaved by a furin-like protease generating the S1 and S2 subunits during trafficking through the Golgi, and at a second site (S2') that primes the protein for fusion with the host cell (23). The S protein of the mutant virus with a HD replacement in the E protein (IBV-EG3) is subject to further proteolysis near the junction of the protein with the viral envelope, resulting in a C-terminal fragment we term the 'stub' (Figure 1A) (15). To compare the processing of the S protein in virions from cells infected with WT-IBV or IBV-EG3, supernatants from cells infected for 18 h at an MOI of 0.05 were clarified and virions were enriched by spinning through a 20% sucrose cushion. The pellets were subjected to SDS-PAGE and immunoblots were probed with a monoclonal antibody that recognizes S1 (3C7B8, (24)), and a polyclonal antibody raised to the C-terminus of S that detects S2 fragments, including the stub (25). As shown in Figures 1B and 1C, EG3 virions have significantly less S1 than WT virions, with an increased fraction of a fragment that runs at about 65 kDa. EG3 virions also have reduced S2 and increased S2' and stub compared to WT virions. We previously reported that nearly all of the S in purified EG3 virions was cleaved to the stub (15). We believe the additional cleavage in the purified virus occurred during isolation as the multiple steps (including two sucrose gradients) were performed in the absence of protease inhibitors, unlike the enrichment procedure described here. These results suggest that IBV-EG3 virus encounters cellular

proteases more readily than WT virus, or that the S protein undergoes a conformational change that is more conducive to processing during trafficking of virions.

IBV induces an increase in Golgi luminal pH during infection. One possible explanation for the aberrant processing of S in IBV-EG3 infected cells is that the microenvironment of the secretory pathway is altered when the E viroporin activity is normal (14, 18, 21), but is unaltered in IBV-EG3 infected cells. Given that the effects of IBV E overexpression on the Golgi are similar to those in cells where the luminal pH is neutralized (4, 6, 7), we measured the luminal pH of the Golgi complex in IBV-infected Vero cells. We used flow cytometric analysis of a ratiometric pHluorin molecule targeted to the Golgi lumen with a reporter consisting of the green fluorescent protein (GFP) pHluorin molecule fused to the membrane targeting sequence of the TGN38 *trans*-Golgi network resident protein (6). We chose to use the *trans*-Golgi network pHluorin because the TGN is the most acidic compartment of the Golgi and thus any alteration in pH would likely be most detectable in this compartment. We generated a clonal Vero cell line that stably expressed pHluorin-TGN38 (Figure 2A). The generation of this cell line allowed us to ensure that all infected cells were expressing pHluorin-TGN38. The cells were treated with cycloheximide for 60 min to chase newly synthesized TGN38-pHluorin from the endoplasmic reticulum (ER). To generate a pH calibration curve, uninfected cells were subjected to treatment with buffers ranging from pH 5.5 to 7.5 in the presence of the ionophores monensin and nigericin prior to flow analysis. The emission ratios of the biphasic pH-sensitive pHluorin at these known pH values can then be used to construct a standard curve (Figure 2B), and predict the Golgi luminal pH in cells infected with IBV in buffer at physiological pH and lacking ionophores (Figure 2C). Infection resulted in a robust increase in the Golgi luminal pH (Figures 2D and 2E).

We attempted to measure the Golgi luminal pH in cells infected with IBV-EG3, but were unable to achieve a high percent of infected cells in the absence of syncytium formation, since

this virus is not efficiently released and spreads best by cell-cell fusion. We found that syncytia were fragile, and this precluded flow cytometric analysis. Instead we turned to transfected cells to determine if the E protein could neutralize the Golgi lumen.

Overexpression of the IBV E protein increases the pH of the Golgi lumen. To determine if the E protein was responsible for the pH change, HeLa cells were co-transfected with a plasmid encoding IBV E along with pHluorin-TGN38, or with the pHluorin-TGN38 alone. We used transient transfection of the reporter here to ensure the pHluorin expressing cells were also expressing the E protein, and used HeLa cells for their ease of transfection. In separate cells, we included a plasmid encoding IBV M (as another overexpressed Golgi membrane protein) as a control. As described above, transfected cells were pretreated with cycloheximde for 60 min to chase newly synthesized proteins out of the ER. A standard curve in cells expressing pHlorin-TGN38 alone was produced in cells treated with ionophores in calibrated pH buffers (Figs 3A and B) as described above. As shown in Figures 3C and D, IBV E robustly neutralized the *trans*-Golgi luminal pH when over expressed in HeLa cells, whereas overexpression of the IBV M protein did not.

The increase in Golgi pH correlates with the LMW pool of IBV E. To determine the role of IBV E oligomerization and by inference viroporin activity in the alteration of Golgi luminal pH, we analyzed two HD point mutants of IBV E that segregate into different oligomeric states. Our previous findings suggest that IBV E^{A26F} is found predominantly in the LMW, likely monomeric form, and IBV E^{T16A} is found predominantly in the HMW, higher-order oligomer (21). In addition, we analyzed the EG3 mutant of IBV E, with a complete HD replacement. Both IBV E^{T16A} and IBV EG3 had *trans*-Golgi pH measurements similar to the IBV M membrane protein control (pH 6.95 and pH 6.87, respectively), while IBV E^{A26F} elicited a pH increase similar to that of the wild-type IBV E protein (pH 7.18, Figure 4A.) This suggested that the LMW pool of IBV E correlates

with the luminal pH increase of the Golgi in addition to the secretory pathway disruption demonstrated in our previous work (14, 18, 21). The same experiment was performed with a *medial*-Golgi pHluorin, GnT1-pHluorin (GnT1, N-acetylglucosaminyltransferase I), to assess if the alteration in pH was specific to the TGN. Here the standard curve was generated from cells expressing GnT2-pHlorin alone. Expression of either IBV E or IBV E^{A26F} elicited a robust pH increase (Figure 4B). Interestingly, IBV E^{T16A} increased the pH significantly, though not as robustly as IBV E and IBV E^{A26F}. We found that the pH of the *trans*-Golgi (measured with pHluorin-TGN38) was higher than the *medial*-Golgi (measured with GnT1-pHluorin). This was unexpected and is addressed in the Discussion. We previously reported that the T16A mutant was not completely inactive in Golgi disruption (21), and the better dynamic range of the *medial*-Golgi pHluorin is likely the reason we were able to measure a significant increase at the *medial*-Golgi but not in the TGN. Altogether, the results in transfected cells implicate the monomeric form of IBV E in neutralization of the Golgi lumen during infection and transfection.

Attempts to rescue IBV EG3 by manipulation of Golgi pH. Despite intense efforts we were unable to conclusively determine whether an increase in Golgi pH could rescue the deficiencies of the IBV EG3 virus. We used two different methods to neutralize acidic compartments: drugs (baflinomycin A1, monensin or ammonium chloride), and overexpression of influenza A M2, a pH activated proton channel. However, the drugs inhibited exocytosis at all concentrations used (during short or long infections), including release of virus. For IAV M2 transfection, we were unable to obtain a high percentage of transfected cells that were subsequently infected with IBV-EG3. In several experiments where the percent of transfected and infected cells was greater than 40%, we obtained 40-75% increases in release of infectious IBV-EG3 virus, but most experiments failed to show a reasonable overlap of transfection and infection and rescue of IBV-EG3 infectivity (data not shown). Additionally, attempts to make stable lines expressing M2 and pHluorin-TGN38 did not yield lines expressing M2 at a high enough level to alter Golgi

luminal pH. We thus turned to another approach to assess the role of neutralization of the Golgi by IBV E.

Expression of IAV M2 decreases the total amount of IBV S at the cell surface, and the cleaved S species in cells. We predicted that neutralization of Golgi pH by IBV E during infection protects the IBV S protein from premature proteolysis at the normal acidic pH of the trans-Golgi. We also predicted that processing and trafficking of IBV S in the presence of a protein that can alter pH (i.e. IBV E or IAV M2) would be similar, while one deficient in this (IBV EG3 or E^{T16A}) would produce premature cleavage and more IBV S at the surface of cells. To test these predictions, we first demonstrated that when transiently overexpressed in Vero cells, IAV M2 neutralized the *trans*-Golgi in our pHluorin/ flow cytometry assay in the absence of the M2 inhibitor amantadine, but not in the presence of 5 μM amantadine as expected (Figures 5A and 5B, (5, 9–11)). With proof of principal established for M2 pH alteration during transfection, cells were co-transfected with plasmids encoding IBV S and IBV E, or IBV EG3, with or without the IAV M2 protein. Surface biotinylation was performed, and the level of IBV S at the cell surface after streptavidin pull-down was determined by western blot analysis (Figure 5C). As predicted, there was a significant increase in the total amount of IBV S at the surface of EG3 expressing cells as compared to cells expressing WT IBV E. Notably, the presence of M2 in EG3 expressing cells reduced the amount IBV S at the surface of cells compared to cells transfected with empty vector (Figure 5D). We also measured the total amounts of cleaved IBV S species (S2, S2', and stub) in transfected cell lysates (without surface biotinylation). We only analyzed S2 fragments, since most of the S in transfected cells is S0 and the S1-specific monoclonal antibody signal was too weak to detect S1 and smaller fragments in this assay. The levels of S2 and stub in EG3-expressing cells were significantly reduced when M2 was co-expressed, with an increase in S0 similar to levels in WT E expressing cells (Fig. 6A and 6B). Importantly, aberrant processing of IBV S in cells cotransfected with empty vector or IBV E^{T16A} could be

abrogated by expression of IAV M2 (Figure 6C and 6D). On the other hand, the presence of M2 had no effect on IBV S processing in cells expressing IBV E WT or IBV E^{A26F}, and cells expressing these IBV E constructs always had less S2 and undetectable levels of the stub. These results suggest that neutralizing Golgi luminal pH could indeed reduce trafficking of IBV S to the plasma membrane and protect it from premature cleavage.

Discussion

Neutralization of the Golgi by IBV E. Our flow cytometry and pH sensitive ratiometric analysis demonstrated that the Golgi luminal pH is increased in IBV infected cells. Overexpression of IBV E caused a similar increase in the pH of the lumen of the *trans*-Golgi and also increased the pH of the *medial*-Golgi. Our baseline measurement of pH 6.78 in the context of transient overexpression of the TGN38-pHluorin and IBV E protein in HeLa cells (Figure 3D), and the baseline of 6.76 in the context of Vero cells stably expressing the TGN38-pHluorin (Figure 2E) are both similar, though somewhat higher, than pH values reported in the literature for the TGN. Values for the pH reported by pHluorin-TGN38 in different cell types range from pH 6.2-6.7 (6, 26, 27). We believe that the higher baseline measurement we observed is likely due to some plasma membrane cycling of pHluorin-TGN38, which would increase the average pH in a given cell since the pH of the extracellular buffer was pH 7.3. The cycling of pHluorin-TGN38 is likely to be the predominant reason for a higher than expected TGN pH, since the *medial*-Golgi pHluorin reported a pH of ~6.4 (Figure 4B). We believe that the consistent shift in the Golgi pH in cells expressing IBV E is more important than the actual baseline pH value we observed with the pHlorin-TGN38. Previously, the TGN38-pHluorin construct was used to demonstrate that CHO cells lacking the counter-ion channel Golgi pH regulator (GPHR) had a 0.4 pH unit increase (6), which substantiates the magnitude of the observed pH increase in this study.

Neutralization of Golgi luminal pH correlates with secretory pathway disruption and the LMW pool of IBV E. Our analysis of the HD mutants of IBV E demonstrated that neutralization of the TGN induced by overexpression of wild-type IBV E correlates with the presence of the LMW, likely monomeric, pool of IBV E, which is the predominant form of the protein observed in cells expressing the IBV E^{A26F} mutant (Figure 4). The IBV E^{A26F} mutant elicited a pH shift slightly higher than the increase observed with the WT IBV E protein. However, the IBV E^{T16A} or IBV EG3 HD mutants did not cause a statistically significant pH shift in the *trans*-Golgi lumen. We previously showed that the LMW pool of IBV E correlates with the secretory pathway disruption (21), including Golgi disassembly and slow trafficking of model cargo proteins, observed when the wild-type IBV E protein is expressed (14, 18). We hypothesized that the Golgi disruption was likely occurring in an IBV E ion channel-independent manner (21). This study corroborates our hypothesis and suggests that the monomeric form of IBV E causes Golgi disruption via alteration of Golgi luminal pH through a mechanism involving interaction with a host protein. This interpretation is strengthened by evidence demonstrating that neither the IBV E^{T16A} or IBV E^{A26F} mutants have ion channel activity in artificial membranes (22), suggesting that any remaining HMW, oligomeric IBV E that may be present when IBV E^{A26F} is expressed is not likely eliciting secretory pathway disruption or pH neutralization via IBV E ion channel activity. However, To *et al.* recently reported that mutation of IBV E at T16 but not A26 prevents oligomerization of IBV E, the opposite of our findings (22). The difference in these results is likely due to different modes of protein expression and the downstream assays used to evaluate oligomerization. In our studies we expressed the HD mutants in mammalian cells and evaluated oligomerization via velocity sucrose gradient analysis followed by cross-linking and immunoprecipitation of gradient fractions of interest (21). To *et al.* bacterially expressed these proteins and then analyzed them via native PAGE electrophoresis after purifying and resolubilizing the samples (22).

Neutralization of Golgi luminal pH by IBV E and IAV M2 correlates with reduced cleavage of IBV S protein. A current model for the cleavage and function of CoV S proteins suggests that proteolytic processing at two cleavage sites (S1/S2 and S2') releases the protein from its pre-fusion conformation and allows exposure of the fusion peptide (28, 29). This change in conformation may also release the S1 subunits from the S2 subunits of the CoV S trimer (28). A possible detrimental consequence of the normal acidic Golgi pH to the virus could be that the S protein is subject to a conformational change and premature and possibly excessive proteolytic processing, resulting in release of the S1 subunit prior to receptor binding. This would result in noninfectious or impaired virions. Indeed, the level of S1 in EG3 virions is lower than in WT virions compared to the level of total S2 (Figure 1B). Our data also indicate that when IBV S is expressed in cells alone or in the presence of EG3 or IBV E^{T16A}, the levels of IBV S cleavage species are increased significantly as compared to IBV S in the presence of IBV E, IBV E^{A26F} or IAV M2, lending support to the hypothesis that the neutralization of Golgi pH by IBV E protects IBV S from premature cleavage (Figure 6). Additionally, when overexpressed in cells with EG3, S is present to a greater extent at the cell surface compared to when expressed with WT E Figure 5D), corroborating previous data observed during IBV EG3 infection (14).

CoV E protein viroporins and host protein interaction. The finding that IBV E modifies the luminal microenvironment to promote infectious virus production indicates similarities to IAV M2 and HCV p7. What is strikingly different about IBV E however, is that this protein is likely causing secretory pathway disruption in an IBV E ion channel-independent way. If IBV E were acting as a monomer to elicit secretory pathway disruption and alter pH, interaction of IBV E with a host protein(s) would be necessary.

Evidence suggests that CoV E proteins interact with host cell proteins to influence pathogenicity (30). Interaction of SARS-CoV E with the PDZ (post-synaptic density protein-95/discs Large/zonula occludens-1) domain containing scaffolding protein, syntenin, and with

the tight junction protein PALS1 (protein associated with Lin Seven 1) through its PBM (PDZ-binding motif) domain, implicates the E protein as a pathogenic determinant (31–33). Our study suggests that the transmembrane domain of IBV E might interact with a transmembrane host protein to induce a pH increase in the Golgi lumen (e.g. by altering the activity of the vATPase, or the proton leak channel or a channel that relieves membrane potential (4)). It is also possible that the relatively long cytoplasmic tail of IBV E interacts with a host protein to modify the secretory pathway. In this case, alterations in the HD could lead to structural changes in the cytoplasmic tail that impact such interactions

SARS-CoV 3a and 8a proteins have been shown to have ion-channel activity in artificial membranes in addition to E (31, 34–36). Intriguingly, the SARS-CoV 3a protein elicits inflammatory signaling similar to the SARS-CoV E protein, suggesting that CoVs may encode accessory proteins that i) may overlap in function to the E protein or ii) that may substitute for a particular role of the multifunctional IBV E protein. Additionally, the SARS-CoV 3a protein has been show to induce Golgi fragmentation as an antagonist to the Arf1 GTPase involved in maintaining the structure and function of the Golgi (37). Further study of these SARS-CoV viroporins outside the complicated context of infection, especially their ability to induce pH changes in the lumen of the secretory pathway, will inform our studies on the IBV E protein.

Our results are the first demonstration that the luminal microenvironment of the Golgi is altered by coronavirus infection. While other viral viroporins (e.g. IAV M2 and HCV p7) have been shown to alter the luminal microenvironment, IBV E appears to do so by a mechanism that does not involve its ion channel activity. Whether the role of putative IBV E interacting protein(s) is pH maintenance, vesicle formation, membrane architecture, protein glycosylation or any number of jobs performed by constituents of the secretory pathway, interaction of the protein(s) or lipid(s) with the large amount of IBV E known to reside at the ERGIC could disrupt the pH directly or indirectly by interfering with normal secretion or architecture of the Golgi. In summary, studies addressing CoV E protein-protein and protein-lipid interactions, and the development of

371 tools to evaluate ion-channel activity *in vivo*, will go a long way in elucidating the precise
372 mechanisms of the multifunctional family of viroporin proteins.
373
374 **Materials and Methods**
375 **Cell Culture.** HeLa and Vero cells were cultured in Dulbecco's modified Eagle medium
376 (DMEM; Invitrogen/Gibco, Grand Island, NY) containing 10% fetal bovine serum (FBS; Atlanta
377 Biologicals, Lawrenceville, GA) and 0.1 mg/ml Normocin (Invivogen, San Diego, CA) at 37˚C
378 under 5% CO_2.
379 **Plasmids.** The pCAGSS IBV E, IBV EG3, IBV M, IBV E^{T16A}, IBV E^{A26F}, codon optimized IBV
380 S, M2 and empty pCAGGS-MCS plasmids have been previously described (14, 18, 21, 38–40).
381 The pCAGGS M2 plasmid was a generous gift from Dr. Andrew Pekosz. The pME-zeo-
382 pHluorin-TGN38 plasmid and GnT1-pHluorin plasmids have been previously described and
383 were generous gifts from Dr. Yusuke Maeda (6).
384 **Antibodies.** The rabbit polyclonal antibodies recognizing the C-terminus of IBV E and the N-
385 terminal head of golgin-160 have been previously described (41, 42). The antibody generated to
386 the C-terminus of IBV S (anti-IBV S_{CT}) has also been described (25). The mouse monoclonal
387 antibody recognizing IBV S1 was a gift from Ellen Collisson (24). The mouse monoclonal
388 antibody recognizing the N-terminus of influenza A M2 has been previously described and was
389 a generous gift from Dr. Andrew Pekosz (43). The mouse anti-GFP antibody was from Roche
390 (Mannheim, Germany). The rabbit anti-GFP antibody was from Thermo Fisher Scientific
391 (Rockford, IL). Alexa-Fluor 488-conjugated anti-rabbit IgG, Alexa-Fluor 488-conjugated anti-
392 mouse IgG, Alexa Fluor 568-conjugated anti-rabbit IgG, and Alexa Fluor 568-conjugated anti-
393 mouse IgG were from Invitrogen/Molecular Probes (Eugene, OR).
394 **Transient transfection.** X-tremeGENE 9 DNA Transfection Reagent (Roche, Indianapolis,
395 IN) was used to transiently transfect cells according to the manufacturer's protocol. For the pH
396 measurement experiments subconfluent HeLa cells in 6 mm dishes were transfected with 1 µg

of each plasmid indicated for a particular experiment, diluted into Opti-MEM (Invitrogen/Gibco) with a 1:3 ratio of X-tremeGENE 9. When the TGN38-pHluorin plasmid was transfected alone the pCAGGS-MCS empty vector was transfected to control for the total amount of DNA transfected. For the co-transfection of IBV S with E, EG3 and IAV M2, subconfluent Vero cells in 6 well dishes were transfected with a total of 2 ug of DNA: 1 ug of pCAGGS/IBV S plus 0.5 ug pCAGGS/IBV E or EG3, and 0.5 ug pCAGGS/MCS or pCAGGS/IAV M2 as described above.

Establishment of TGN38-pHluorin stable Vero cell line. Subconfluent Vero cells were transfected with the pME-zeo-pHluorin-TGN38 plasmid according to the manufacturer's protocol (X-tremeGENE 9). Transfected cells were grown in DMEM containing 10% FBS under selection with Zeocin (Invitrogen) at 250 µg/ml. Individual clones were selected and evaluated by indirect immunofluorescence microscopy.

IBV S processing in virions. The Beaudette strain of recombinant IBV used in this study, and the IBV-EG3 mutant have been previously described (15, 44). Confluent Vero cells in 35 mm dishes were infected at a MOI of 0.05 with wild-type IBV or IBV-EG3 for 18 h. Supernatants (2 ml) were mixed with protease inhibitor cocktail (Sigma), and clarified by centrifugation at 4K RPM for 20 min at 4^{o}C. Clarified supernatant was overlaid onto a 1 ml sucrose cushion (20% sucrose in 0.15 M NaCl, 10 mM Hepes pH 7.2) in TLA110 centrifuge tubes (Beckman). After spinning at 80K RPM for 60 min, pellets were resuspended in 20 ul of 2X NUPAGE sample buffer containing 5% β-mercaptoethanol, and heated at 90^{o}C for 5 min. Samples were electrophoresed in NUPAGE 4-12% gradient gels (ThermoFisher) and transferred to low fluorescence PVDF (Millipore). After blocking in 10 mM Tris-HCl pH 7,4, 0.15 M NaCl (TBS) plus 5% nonfat milk, membranes were probed with a mouse monoclonal antibody (3C7B8) for 2-3 days at 4^{o}C to detect S1-containing fragments. After rinsing in TBS/0.05% Tween 20 (TBST), S2-containing fragments were detected with rabbit anti-IBV S_{CT} (25) diluted 1:3000 in TBST/milk for 1 h at RT. Secondary antibodies were donkey anti-mouse IgG-800 and donkey anti-rabbit IgG-680 (both from LI-COR), diluted 1:10,000 in TBST/milk. Blots were imaged using

the LI-COR Odyssey CLx at 700 and 800 nm wavelengths. Quantification was performed in Image Studio (LI-COR), and each IBV S fragment was expressed as the percent of the total S. Statistical analysis was in Prism-GraphPad.

Indirect immunofluorescence microscopy. Cells were washed with phosphate-buffered saline (PBS) and fixed in 3% paraformaldehyde in PBS for 10 min at 22˚C. The fixative was quenched in PBS containing 10 mM glycine (PBS-Gly), and the cells were permeabilized in 0.5% Triton X-100 in PBS-Gly for 3 min. The coverslips were washed twice with PBS-Gly and incubated in primary antibody in PBS-Gly with 1% BSA for 20 min at room temperature. Rabbit anti-IBV E and rabbit anti-golgin160 were used at 1:1,000. Rabbit anti-GFP and mouse anti-M2 were used at 1:500. Mouse anti-GFP was used at 1:300. The cells were then washed twice with PBS-Gly and incubated for 20 min in secondary antibody diluted in PBS-Gly with 1% BSA. Alexa-Fluor 488-conjugated anti-rabbit IgG and Alexa Fluor 568-conjugated anti-mouse IgG were used at 1:1,000. The coverslips were washed twice in PBS-Gly and incubated with Hoescht 33285 [0.1 µg/ml] to stain DNA, rinsed twice in PBS-Gly and mounted on slides in glycerol containing 0.1M *N*-propylgallate. Images were captured using an Axioskop microscope (Zeiss) equipped for epifluorescence with an ORCA-03G charge-coupled-device camera (Hamamatsu, Japan) and iVision software (Bio Vision Technologies).

Determination of Golgi pH during IBV infection. Vero cells stably expressing TGN38-pHluorin, seeded on 6 cm dishes at 3.5×10^5, were inoculated with IBV diluted to an MOI of 25 in serum-free (SF) DMEM, and virus was adsorbed for 1 h with rocking. Inoculum was removed, and the cells were rinsed with DMEM containing 5% FBS. The cells were then incubated at 37˚C in DMEM containing 5% FBS for 18 h. Cells were washed with PBS and trypsinized for 3 min and resuspended in ice cold SF DMEM. Cells were centrifuged at 112 × g and washed with ice cold SF DMEM twice. Cells were centrifuged as above and resuspended in 1 ml of the calibration buffers (140 mM KCl, 2 mM $CaCl_2$, 1mM $MgSO_4$, 1.5 mM K_2HPO_4, 10 mM glucose, 10 mM MES, 10 mM HEPES, 10 µM monensin, 10 µM nigericin) of specified pH to generate a

449 calibration curve, or Na-RINGER Buffer pH 7.3 (140 mM NaCl, 2 mM $CaCl_2$, 1mM $MgSO_4$, 1.5
450 mM K_2HPO_4, 10 mM glucose, 10 mM MES, 10 mM HEPES) in the case of experimental
451 samples. The cells were incubated at room temperature for ~10 min before being run through a
452 Becton Dickinson LSRII flow cytometer. The pHluorin was excited at 405 nm and 488 nm and
453 the emission signals were collected with detection filters at 500-550 nm and 515-545 nm,
454 respectively. Flow cytometric data was collected and quantified using FACS Diva software 8.0.
455 The emission ratios (405:488) of TGN38-pHluorin in calibration buffers of known pH were used
456 to generate a linear calibration curve (Microsoft Excel) with which to calculate the luminal Golgi
457 pH in infected and uninfected cells.

458 **Transient expression of TGN38-pHluorin or GnT1-pHluorin and IBV E or HD mutants in**
459 **HeLa cells.** At 12 h post-transfection, HeLa cells transiently expressing wild-type (WT) or
460 mutant IBV E and TGN38-pHluorin or GnT1-pHluorin, or TGN38-pHluorin alone or GnT1-
461 pHluorin alone, were washed with serum-free (SF) DMEM and incubated for 1 h at 37˚C in SF
462 DMEM containing 100 µg/ml cycloheximide. Cells were then washed with phosphate buffered
463 saline (PBS) and trypsinized for 3 min and resuspended in ice cold SF DMEM. Cells were
464 centrifuged at 112 × g and washed with ice cold SF DMEM twice. Cells were centrifuged as
465 above and resuspended in 1 ml of the calibration buffers to generate the standard curve as
466 described above, or in buffer lacking the ionophores to determine the Golgi pH. IBV M, another
467 viral membrane protein localized to the Golgi, was used as a membrane protein overexpression
468 control.

469 **Surface biotinylation.** At 24h post-transfection, Vero cells in 35 mm dishes expressing IBV
470 S with either WT IBV E or EG3, along with either empty vector or IAV M2 were incubated with
471 0.5 mg/ml EZ-link-NHS-SS-biotin (Pierce) in Hank's buffered salt solution at 0^{o}C for 30 min.
472 After quenching the biotin in PBS with 10 mM glycine for 5 min at 0^{o}C, cells were rinsed in PBS,
473 scraped into PBS and pelleted at 4K RPM for 2.5 min. After lysis in 60 ul of detergent solution
474 [1% NP40, 0.4% deoxycholate, 50 mM Tris-HCl pH 8.0, and 62.5 mM EDTA plus protease

inhibitor cocktail] at 0°C for 20 min, samples were clarified by spinning at 14K RPM for 10 min at 4°C. Ten percent (6 ul) was removed for "input" (and combined with 6 ul of 2X sample buffer) and the remainder was diluted with 200 ul NHN (1% NP40, 10 mM Hepes pH 7.2, 150 mM NaCl). Streptavidin-agarose beads (50 ul of a 50% slurry, Pierce) washed in NHN were added and samples were incubated for 2h at 4°C and 30 min at 22°C. The beads were washed twice in NHN and eluted in 2x sample buffer and electrophoresed and transferred to PVDF as described above. S2-containing fragments were detected with rabbit anti-S_{CT} and donkey anti-rabbit IgG-680 and quantified as described above.

Assessment of IBV S proteolytic processing in transfected cells. Subconfluent Vero cells in 35 mm dishes were transfected with 1 ug of plasmid encoding IBV S alone or with 0.5 ug of a plasmid encoding IBV E, EG3, T16A or A26F, with or without 0.5 ug of a plasmid encoding IAV M2 as described above. Total DNA in each transfection was adjusted to 2 ug with empty vector. Cells were lysed in 100 ul of detergent solution (as described above) at 21-24h post-transfection. Approximately 15% of each sample was resolved by SDS-PAGE, transferred to PVDF and blotted as described above. IBV S2 fragments were detected with anti-S_{CT} . Equivalent samples were run on a separate gel to detect IBV E (rabbit anti-IBV E) and IAV M2 (mouse anti-M2).

Acknowledgements

We thank Helene Verhije (Utrecht University) for plasmids used in the construction of the codon-optimized IBV S construct, Ellen Collison and Yvonne Drechsler (Western University of Health Sciences) for the monoclonal anti-IBV-S1, Yusuke Maeda (Osaka University) for the pHlorin-TGN38 and GnT1-pHlorin plasmids, and Andrew Pekosz (The Johns Hopkins Bloomberg School of Public Health) for the M2 expression construct and antibody. We also thank Tricia Nilles for help with flow cytometry and the past and present members of the Machamer lab for

critical and helpful discussions about the data presented here. This work was supported by NIH R01 GM117399 and NIH T32 GM007445.

References

1. Menachery VD, Graham RL, Baric RS. 2017. Jumping species—a mechanism for coronavirus persistence and survival. Curr Opin Virol 23:1–7.
2. Channappanavar R, Zhao J, Perlman S. 2014. T cell-mediated immune response to respiratory coronaviruses. Immunol Res 59:118–128.
3. Hogue BG, Machamer CE. 2008. Coronavirus Structural Proteins and Virus Assembly, p. 179–200. *In* Perlman, S, Gallagher, T, Snijder, E (eds.), Nidoviruses. American Society of Microbiology.
4. Weisz OA. 2003. Acidification and protein traffic. Int Rev Cytol 226:259–319.
5. Sakaguchi T, Leser GP, Lamb RA. 1996. The ion channel activity of the influenza virus M2 protein affects transport through the Golgi apparatus. J Cell Biol 133:733–47.
6. Maeda Y, Ide T, Koike M, Uchiyama Y, Kinoshita T. 2008. GPHR is a novel anion channel critical for acidification and functions of the Golgi apparatus. Nat Cell Biol 10:1135–45.
7. Mollenhauer HH, Morré DJ, Rowe LD. 1990. Alteration of intracellular traffic by monensin; mechanism, specificity and relationship to toxicity. Biochim Biophys Acta 1031:225–46.
8. Scott C, Griffin S. 2015. Viroporins: structure, function and potential as antiviral targets. J Gen Virol 96:2000–2027.
9. Sugrue RJ, Bahadur G, Zambon MC, Hall-Smith M, Douglas AR, Hay AJ. 1990. Specific structural alteration of the influenza haemagglutinin by amantadine. EMBO J 9:3469–3476.
10. Steinhauer D a, Wharton S a, Skehel JJ, Wiley DC, Hay a J. 1991. Amantadine selection of a mutant influenza virus containing an acid-stable hemagglutinin glycoprotein:

evidence for virus-specific regulation of the pH of glycoprotein transport vesicles. Proc Natl Acad Sci U S A 88:11525–11529.

11. Ciampor ' F, Thompson ' CA, Grambas S, Hay AJ, Ciampor F, Thompson CA, Grambas S, Hay AJ. 1992. Regulation of pH by the M2 protein of influenza A viruses. Virus Res 22:247–258.

12. Wozniak AL, Griffin S, Rowlands D, Harris M, Yi M, Lemon SM, Weinman SA. 2010. Intracellular proton conductance of the hepatitis C virus p7 protein and its contribution to infectious virus production. PLoS Pathog 6:e1001087.

13. Bentham MJ, Foster TL, McCormick C, Griffin S. 2013. Mutations in hepatitis C virus p7 reduce both the egress and infectivity of assembled particles via impaired proton channel function. J Gen Virol 94:2236–2248.

14. Ruch TR, Machamer CE. 2011. The Hydrophobic Domain of Infectious Bronchitis Virus E Protein Alters the Host Secretory Pathway and Is Important for Release of Infectious Virus. J Virol 85:675–685.

15. Machamer CE, Youn S. 2006. The transmembrane domain of the infectious bronchitis virus E protein is required for efficient virus release. Adv Exp Med Biol 581:193–8.

16. Corse E, Machamer CE. 2002. The cytoplasmic tail of infectious bronchitis virus E protein directs Golgi targeting. J Virol 76:1273–84.

17. Corse E, Machamer CE. 2003. The cytoplasmic tails of infectious bronchitis virus E and M proteins mediate their interaction. Virology 312:25–34.

18. Ruch TR, Machamer CE. 2012. A single polar residue and distinct membrane topologies impact the function of the infectious bronchitis coronavirus E protein. PLoS Pathog 8:e1002674.

19. Nieto-Torres JL, DeDiego ML, Verdiá-Báguena C, Jimenez-Guardeño JM, Regla-Nava JA, Fernandez-Delgado R, Castaño-Rodriguez C, Alcaraz A, Torres J, Aguilella VM, Enjuanes L. 2014. Severe acute respiratory syndrome coronavirus envelope protein ion

channel activity promotes virus fitness and pathogenesis. PLoS Pathog 10:e1004077.

20. Verdia-Baguena C, Nieto-Torres JL, Alcaraz A, DeDiego ML, Torres J, Aguilella VM, Enjuanes L. 2012. Coronavirus E protein forms ion channels with functionally and structurally-involved membrane lipids. Virology 432:485–494.

21. Westerbeck JW, Machamer CE. 2015. A Coronavirus E Protein is Present in Two Distinct Pools with Different Effects on Assembly and the Secretory Pathway. J Virol 89:9313–9323.

22. To J, Surya W, Fung TS, Li Y, Verdià-Bàguena C, Queralt-Martin M, Aguilella VM, Liu DX, Torres J. 2017. Channel-Inactivating Mutations and Their Revertant Mutants in the Envelope Protein of Infectious Bronchitis Virus. J Virol 91:e02158-16.

23. Yamada Y, Liu DX. 2009. Proteolytic activation of the spike protein at a novel RRRR/S motif is implicated in furin-dependent entry, syncytium formation, and infectivity of coronavirus infectious bronchitis virus in cultured cells. J Virol 83:8744–58.

24. Parr RL, Collisson EW. 1993. Epitopes on the spike protein of a nephropathogenic strain of infectious bronchitis virus. Arch Virol 133:369–383.

25. Lontok E, Corse E, Machamer CE. 2004. Intracellular targeting signals contribute to localization of coronavirus spike proteins near the virus assembly site. J Virol 78:5913–22.

26. Miesenböck G, De Angelis DA, Rothman JE. 1998. Visualizing secretion and synaptic transmission with pH-sensitive green fluorescent proteins. Nature 394:192–195.

27. Poschet JF, Boucher JC, Tatterson L, Skidmore J, Van Dyke RW, Deretic V. 2001. Molecular basis for defective glycosylation and Pseudomonas pathogenesis in cystic fibrosis lung. Proc Natl Acad Sci U S A 98:13972–13977.

28. Walls AC, Tortorici MA, Snijder J, Xiong X, Bosch B-J, Rey FA, Veesler D. 2017. Tectonic conformational changes of a coronavirus spike glycoprotein promote membrane fusion. Proc Natl Acad Sci 114:11157–11162.

29. Shang J, Zheng Y, Yang Y, Liu C, Geng Q, Luo C, Zhang W, Li F. 2018. Cryo-EM structure of infectious bronchitis coronavirus spike protein reveals structural and functional evolution of coronavirus spike proteins. PLOS Pathog 14:e1007009.

30. To J, Torres J. 2018. Beyond channel activity: Protein-protein interactions involving viroporins, p. 329–377. *In* Harris J., BD (ed.), Virus Protein and Nucleoprotein Complexes. Subcellular Biochemistryvol 88. Springer, Singapore.

31. DeDiego ML, Nieto-Torres JL, Jimenez-Guardeno JM, Regla-Nava JA, Castano-Rodriguez C, Fernandez-Delgado R, Usera F, Enjuanes L. 2014. Coronavirus virulence genes with main focus on SARS-CoV envelope gene. Virus Res 194:124–137.

32. Teoh K-T, Siu Y-L, Chan W-L, Schluter MA, Liu C-J, Peiris JSM, Bruzzone R, Margolis B, Nal B. 2010. The SARS coronavirus E protein interacts with PALS1 and alters tight junction formation and epithelial morphogenesis. Mol Biol Cell 21:3838–3852.

33. Jimenez-Guardeno JM, Nieto-Torres JL, DeDiego ML, Regla-Nava JA, Fernandez-Delgado R, Castano-Rodriguez C, Enjuanes L. 2014. The PDZ-binding motif of severe acute respiratory syndrome coronavirus envelope protein is a determinant of viral pathogenesis. PLoS Pathog 10:e1004320.

34. Lu W, Zheng B-J, Xu K, Schwarz W, Du L, Wong CKL, Chen J, Duan S, Deubel V, Sun B. 2006. Severe acute respiratory syndrome-associated coronavirus 3a protein forms an ion channel and modulates virus release. Proc Natl Acad Sci U S A 103:12540–12545.

35. Chen CC, Krüger J, Sramala I, Hsu HJ, Henklein P, Chen YMA, Fischer WB. 2011. ORF8a of SARS-CoV forms an ion channel: Experiments and molecular dynamics simulations. Biochim Biophys Acta - Biomembr 1808:572–579.

36. Castaño-Rodriguez C, Honrubia JM, Gutiérrez-Álvarez J, DeDiego ML, Nieto-Torres JL, Jimenez-Guardeño JM, Regla-Nava JA, Fernandez-Delgado R, Verdia-Báguena C, Queralt-Martín M, Kochan G, Perlman S, Aguilella VM, Sola I, Enjuanes L. 2018. Role of severe acute respiratory syndrome coronavirus viroporins E, 3a, and 8a in replication and

pathogenesis. MBio 9:02325-17.

37. Freundt EC, Yu L, Goldsmith CS, Welsh S, Cheng A, Yount B, Liu W, Frieman MB, Buchholz UJ, Screaton GR, Lippincott-Schwartz J, Zaki SR, Xu X-N, Baric RS, Subbarao K, Lenardo MJ. 2010. The Open Reading Frame 3a Protein of Severe Acute Respiratory Syndrome-Associated Coronavirus Promotes Membrane Rearrangement and Cell Death. J Virol 84:1097–1109.

38. Hitoshi N, Ken-ichi Y, Jun-ichi M. 1991. Efficient selection for high-expression transfectants with a novel eukaryotic vector. Gene 108:193–199.

39. Neumann G, Watanabe T, Ito H, Watanabe S, Goto H, Gao P, Hughes M, Perez DR, Donis R, Hoffmann E, Hobom G, Kawaoka Y, Grantham ML, Stewart SM, Lalime EN, Pekosz A, Ciampor F, Thompson CA, Grambas S, Hay AJ, Steinhauer D a, Wharton S a, Skehel JJ, Wiley DC, Hay AJ. 1991. Tyrosines in the influenza A virus M2 protein cytoplasmic tail are critical for production of infectious virus particles. Proc Natl Acad Sci U S A 22:11525–11529.

40. Sisk JM, Frieman MB, Machamer CE. 2018. Coronavirus S protein-induced fusion is blocked prior to hemifusion by Abl kinase inhibitors. J Gen Virol 99:619–630.

41. Corse E, Machamer CE. 2000. Infectious bronchitis virus E protein is targeted to the Golgi complex and directs release of virus-like particles. J Virol 74:4319–4326.

42. Chandran S, Machamer CE. 2008. Acute perturbations in golgi organization impact de novo sphingomyelin synthesis. Traffic 9:1894–1904.

43. Zebedee SL, Lamb RA. 1988. Influenza A virus M2 protein: monoclonal antibody restriction of virus growth and detection of M2 in virions. J Virol 62:2762–2772.

44. Youn S, Leibowitz JL, Collisson EW. 2005. In vitro assembled, recombinant infectious bronchitis viruses demonstrate that the 5a open reading frame is not essential for replication. Virology 332:206–215.

631 **Figure legends**

632 **Figure 1.** The IBV S protein is aberrantly processed in virions from IBV-EG3 infected cells.
633 (A) Cartoon of IBV Beaudette S showing the cleavage sites. The signal sequence (ss), fusion
634 peptide (FP), and transmembrane domain (TMD) are indicated. (B) A representative blot of
635 virions purified from the supernatants of WT IBV or IBV EG3 infected Vero cells by
636 concentration through a sucrose cushion. Pellets were electrophoresed on NUPAGE 4-12%
637 gradient gels and after transfer to PVDF membranes were probed with mouse anti-S1 and
638 rabbit anti-S2 followed by donkey anti-mouse IgG-800 and donkey anti-rabbit IgG-680. The left
639 panel is a merge of the 800 and 680 wavelengths of the LiCOR image showing that the S1 and
640 S2 essentially comigrate on these gradient gels. The middle and right panels show the signal for
641 the S1-specific mouse monoclonal 3C7B8 and the rabbit anti-S C-terminus antibodies,
642 respectively. The cleavage products are indicated, as are the positions of the molecular weight
643 markers (in kDa). (C) Quantification showing the fraction of total S for each S1 fragment (upper
644 graph) or S2 fragment (lower graph). Error bars = S.D; n= 4 (S2 antibody) or 3 (S1 antibody). A
645 paired t-test was performed in GraphPad Prism, with $P<0.05$ (*) where indicated. All other pairs
646 were not statistically significant.
647
648 **Figure 2**. IBV infection alters Golgi pH. (A) Vero cells stably expressing pHluorin-TGN38 were
649 evaluated by indirect immunofluorescence microscopy. Cells were labeled with rabbit anti-
650 golgin160 and mouse anti-GFP, followed by Alexa546 anti-rabbit IgG and Alexa 488 anti-mouse
651 IgG. (B) Vero cells stably expressing pHluorin-TGN38 were used to assess the pH of the *trans*-
652 Golgi by determining the ratio of the pH sensitive dual emission spectrum by flow cytometry.
653 The cells were in buffers of known pH and contained ionophores to equilibrate the extracellular
654 and luminal pH of the Golgi. A representative flow cytometry experiment is graphed. (C)
655 Calibration curves were generated from data like that illustrated in (B), in order to calculate the
656 pH of cells infected with IBV or uninfected cells. The calibration curve pictured was derived from

n=3 independent experiments (~10,000 cells each). Error bars = SEM. (D) The cell emission ratios for Vero cells infected or mock infected with IBV and stably expressing pHluorin-TGN38 from a representative experiment are pictured. (E) The average calculated pH values from n=3 independent experiments (~10,000 cells each) are graphed. Unpaired t-tests were performed in Prism at 99% confidence, with an assumption of equal variance. ***P<0.001. Error bars= SEM.

Figure 3. Overexpression of IBV E alters Golgi pH. (A) The *trans*-Golgi pH in HeLa cells transiently expressing pHluorin-TGN38 was assessed by determining the ratio of the pH sensitive dual emission spectrum by flow cytometry. The cells were in buffers of known pH and contained ionophores to equilibrate the extracellular and luminal pH of the Golgi. A representative flow cytometry experiment is graphed. (B) Calibration curves were generated from data like that illustrated in (A), in order to calculate the pH of cells expressing the pHluorin-TGN38 alone or in combination with IBV E or E mutants.. The calibration curve pictured was derived from n=7 independent experiments (~5,000 cells each). Error bars = SEM. (C) The cell emission ratio for HeLa cells expressing pHluorin-TGN38 alone and with IBV E or IBV M (control) from a representative experiment are pictured. (D) The average calculated pH values from n=3 independent experiments are graphed (~5,000 cells each). Unpaired t-tests were performed in Prism at 99% confidence, with an assumption of equal variance. * P<0.05; ***P<0.001. Error bars= SEM.

Figure 4. Change in Golgi pH correlates with LMW HD mutant of IBV E. (A) HeLa cells transiently expressing pHluorin-TGN38 alone or with IBV E or HD mutants were evaluated by flow cytometry and the average calculated pH values from n=3 independent experiments are graphed (~5,000 cells each). (B) HeLa cells transiently expressing a *medial*-Golgi tagged pHluorin, GnT1-pHluorin, with IBV E or HD mutants were evaluated by flow cytometry and the average calculated pH values from n=3 independent experiments are graphed (~5,000 cells

683 each). Unpaired t-tests were performed in Prism at 99% confidence, with an assumption of
684 equal variance. ** P<0.01; ***P<0.001, ****P<0.0001. Error bars= SEM.
685
686 **Figure 5.** Influenza A M2 alters Golgi pH and reduces IBV S at the surface of EG3-expressing
687 cells. (A) Vero cells expressing pHluorin-TGN38 and M2 were evaluated by indirect
688 immunofluorescence microscopy. Cells were labeled with rabbit anti-GFP and mouse anti-M2,
689 followed by Alexa 488 anti-rabbit IgG and Alexa 546 anti-mouse IgG, and Hoescht stain. Some
690 M2 is present in the Golgi region. (B) Vero cells transiently expressing pHluorin-TGN38 with or
691 without transient expression of IAV M2 and with or without treatment with amantadine (5 μM)
692 were evaluated by flow cytometry. The calculated pH values from a single independent
693 experiment are graphed (~5,000 cells each). (C) A representative blot from Vero cells
694 expressing IBV S with either WT IBV E or EG3, along with either empty vector or IAV M2 after
695 surface biotinylation. Biotinylated proteins were isolated with streptavidin-agarose beads from
696 lysates. Both input (10%) and surface fractions (100%) were subjected to western blot analysis
697 with rabbit anti-IBV S_{CT} followed by donkey anti-rabbit IgG-680. IN = input. The positions of the
698 IBV S2 species are indicated, as are the molecular weight markers in kDa. (D) Quantification of
699 the total IBV S at the cell surface from n=3 experiments. The low percent of surface S is likely
700 due to inefficient biotinylation. One-way ANOVA was performed with GraphPad Prism, * P<0.05
701 when compared to WT E + vector. Error bars = SD.
702
703 **Figure 6**. Expression of IAV M2 corrects aberrant processing of IBV S . (A) A representative
704 blot from Vero cells expressing IBV S with either WT IBV E or EG3, along with either empty
705 vector or IAV M2 showing the S2-containing fragments and the positions of the molecular
706 weight markers (in kDa). Expression of E and EG3 was similar by blotting, as was M2 in the
707 relevant samples (not shown). (B) Quantification of n=7 experiments indicating the fraction of
708 each S2 form; error bars = S.D. (C) A representative blot from Vero cells expressing IBV S

alone or with WT IBV E, IBV E^{T16A}, or IBV E^{A26F}, along with either empty vector or IAV M2 showing the S2-containing fragments and the positions of the molecular weight markers (in kDa). The far right lane is a sample from cells transfected with vector alone to indicate the background with the anti-S_{CT} antibody. (D) Quantification of n=3 experiments indicating the fraction of each S2 form. For both graphs, unpaired t-tests were performed with GraphPad Prism between empty vector and IAV M2 expressing samples for each set: NS, not significant, *p<0.05, ** P<0.01, *** P<0.005, with the colors representing the relevant p value.

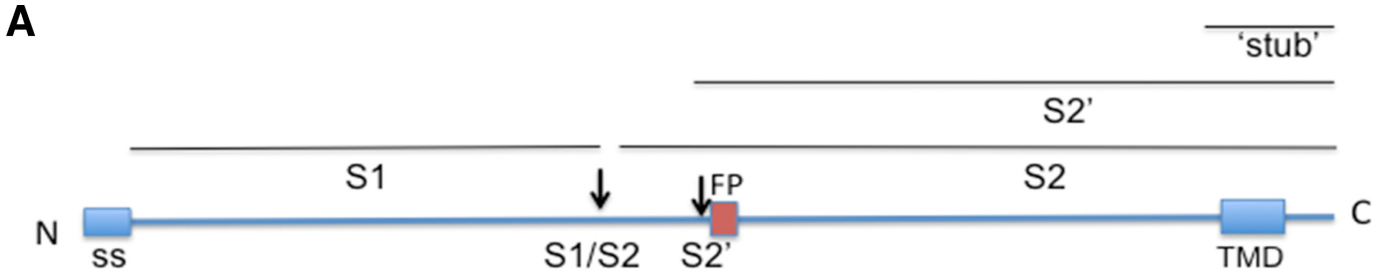

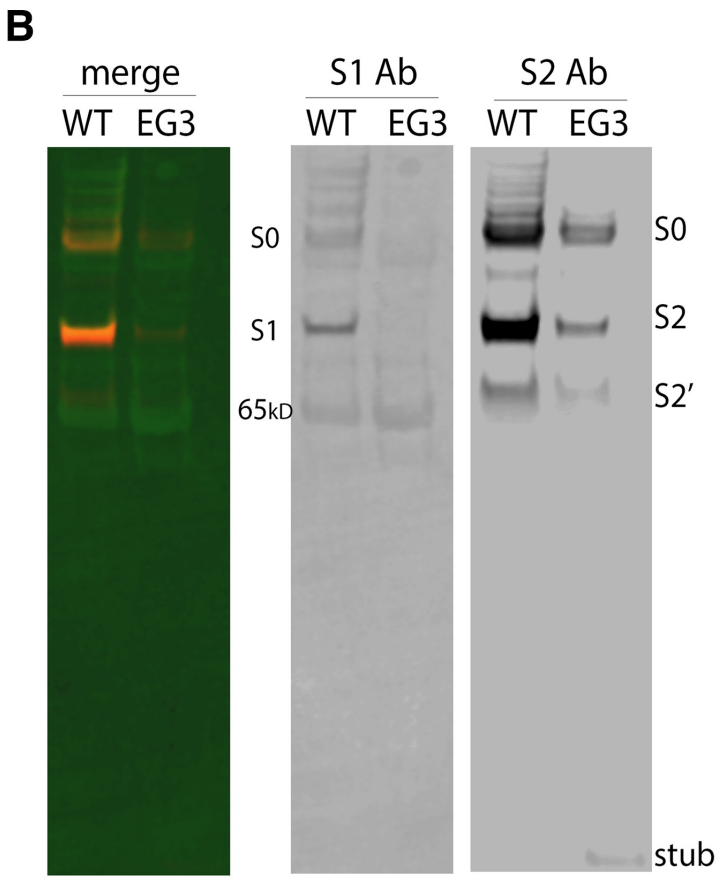

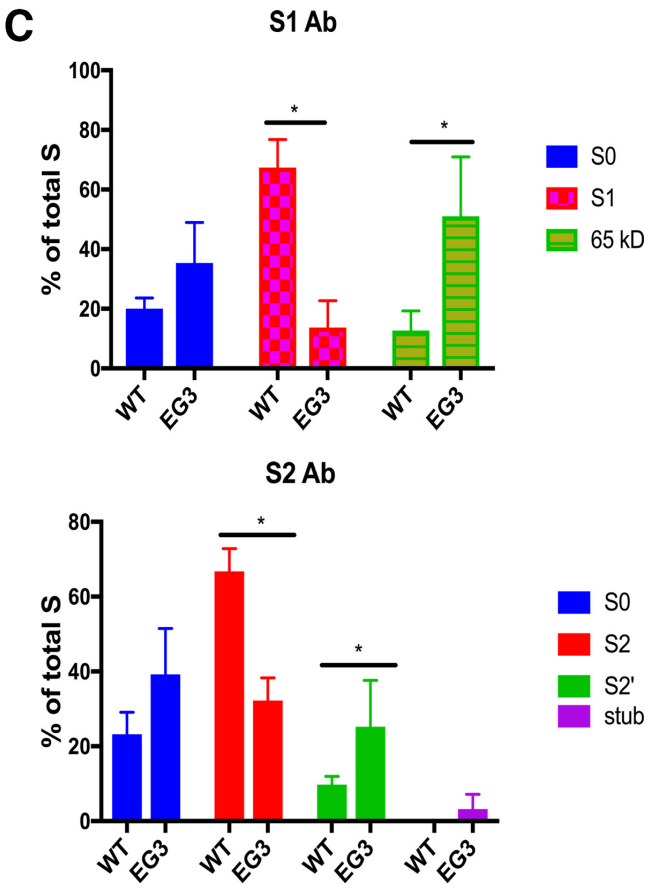

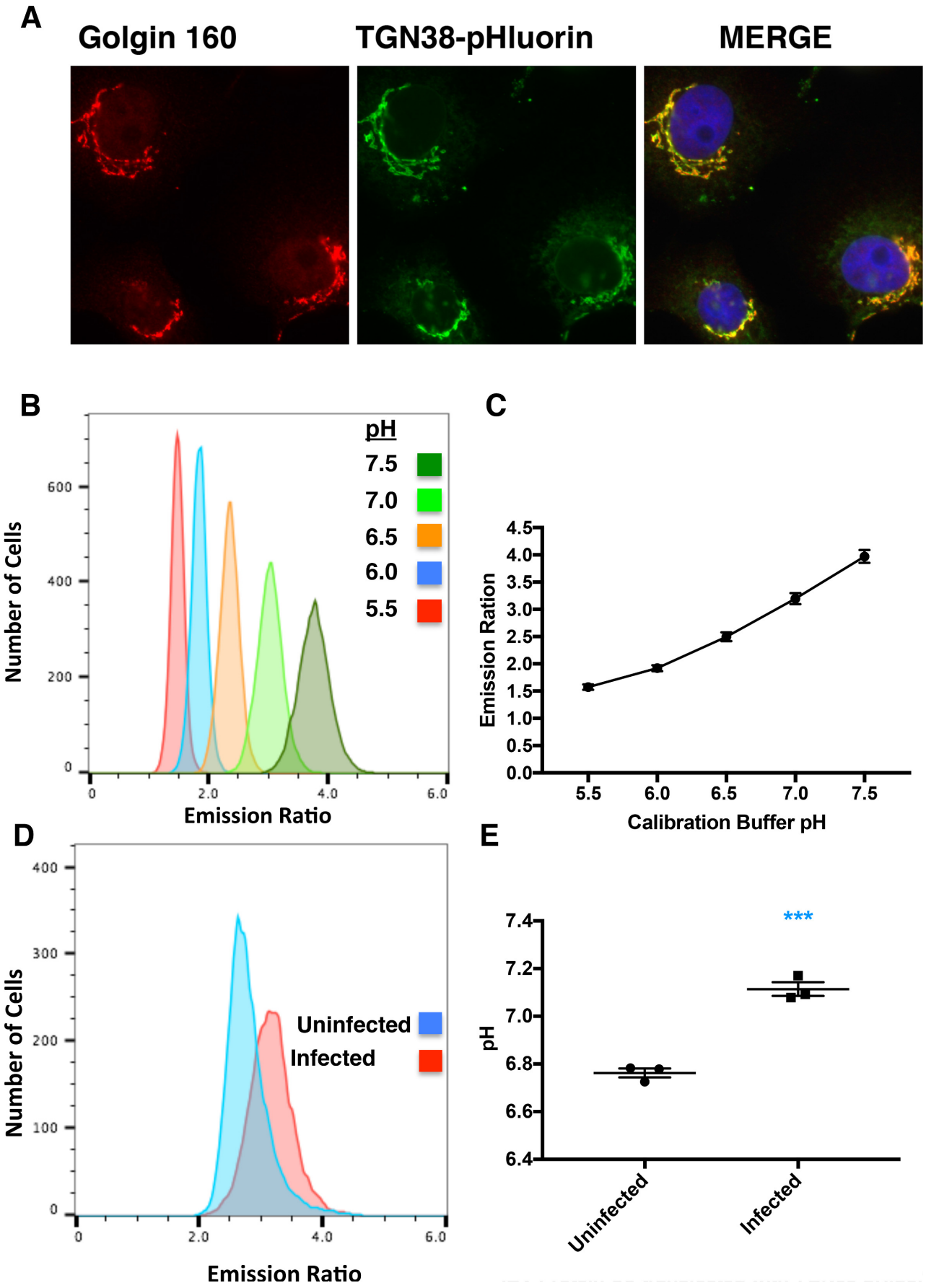

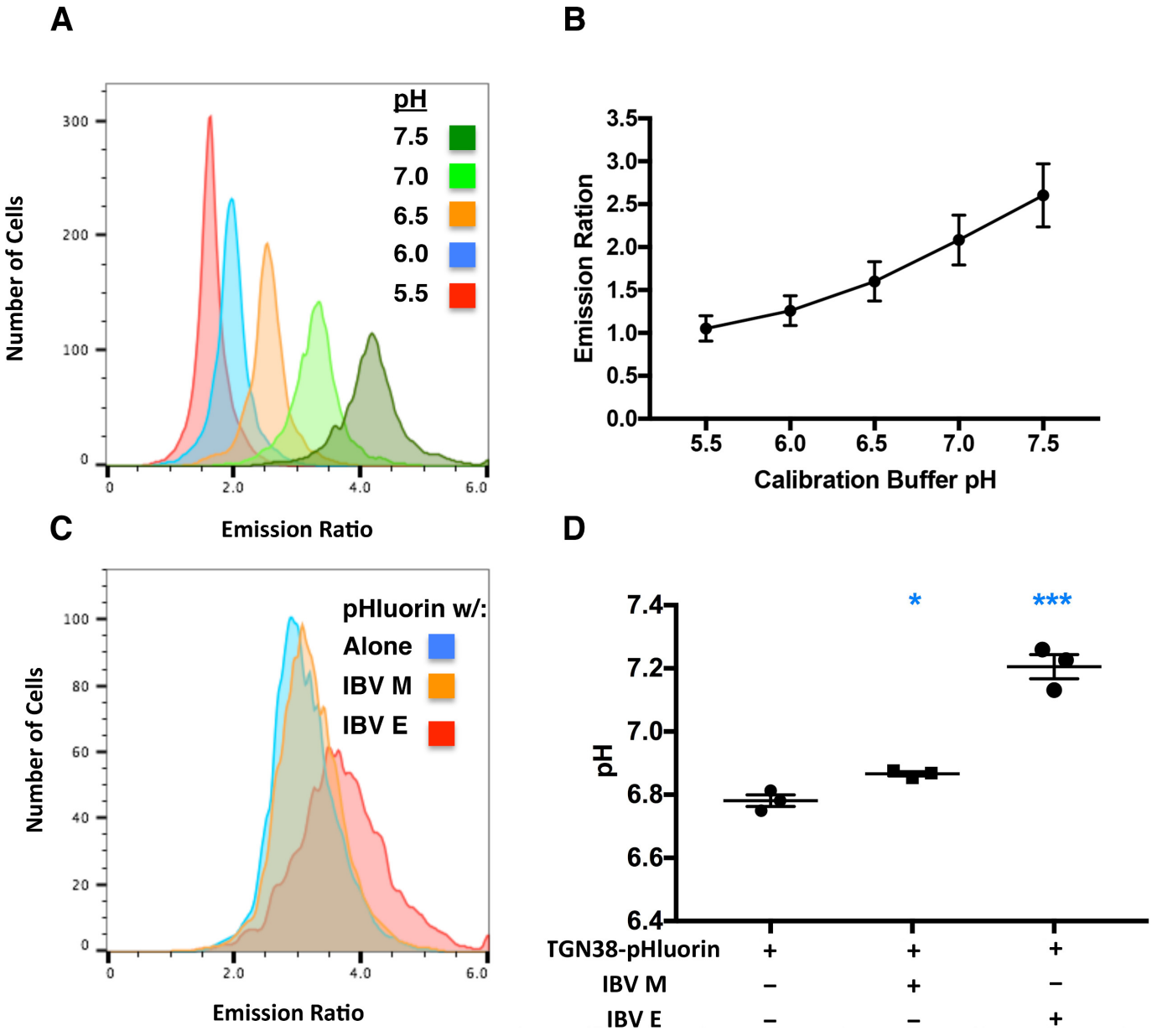

A

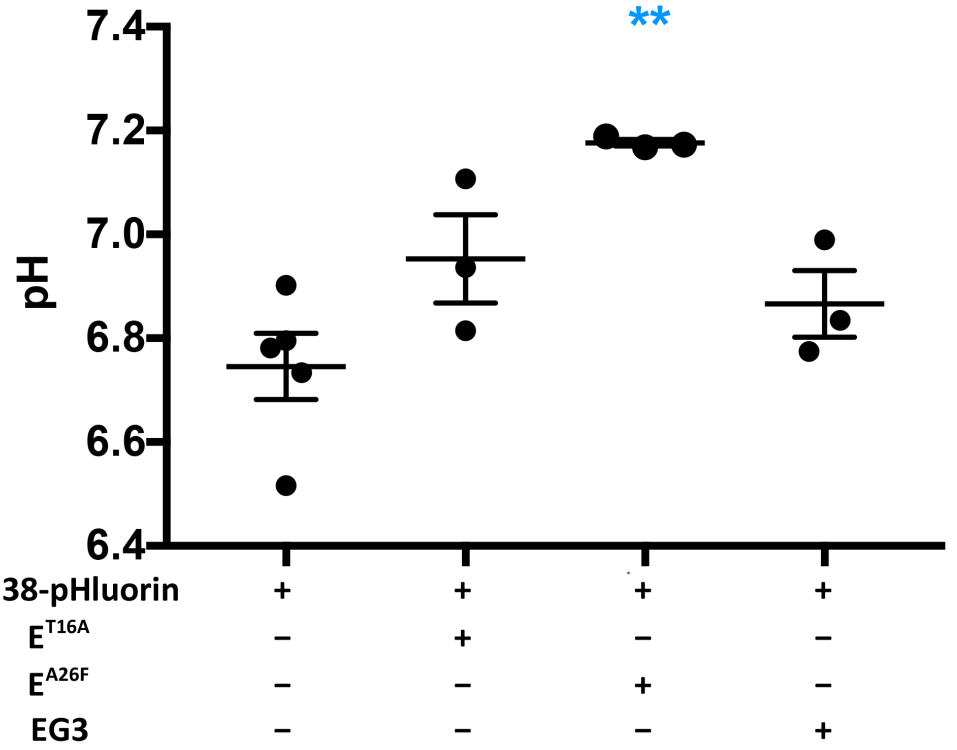

B